Retreat of the Antarctic Ice Sheet during the Last Interglaciation and implications for future change

Nicholas R. Golledge[1,1], Peter U Clark[2,2], Feng He[3,3], Andrea Dutton[4,4], Chris Turney[5,5], Chris Fogwill[6,6], Tim Naish[7,7], Richard H. Levy[8,8], Robert Murray McKay[1,1], Daniel P Lowry[9,9], Nancy A.N. Bertler[1,1], Gavin B Dunbar[1,1], and Anders E. Carlson[10,10]

[1]Victoria University of Wellington
[2]Oregon State University
[3]University of Wisconsin-Madison
[4]University of Florida
[5]University of New South Wales
[6]Keele University
[7]Antarctic Research Centre, Victoria Univ. of Wellington
[8]Geological and Nuclear Sciences - Te Pu Ao
[9]GNS Science
[10]Oregon Glaciers Institute

November 30, 2022

Abstract

The Antarctic Ice Sheet (AIS) response to past warming consistent with the 1.5–2°C 'safe limit' of the United Nations Paris Agreement is currently not well known. Empirical evidence from the most recent comparable period, the Last Interglaciation, is sparse, and transient ice-sheet model simulations are few and inconsistent. Here we present new results from transiently-forced ice-sheet modelling experiments. We evaluate our results against near and far-field proxy reconstructions and find good agreement. Our simulations indicate that the AIS contributed approximately 4 m to global mean sea level, peaking at 126 ka BP, with ice lost primarily from the Amundsen but not Ross or Weddell Sea sectors. The AIS thinned in the area of the Wilkes Subglacial Basin but did not retreat. Continuing beyond present day our model predicts that the West Antarctic Ice Sheet may already be predisposed to collapse even in the absence of further environmental change.

Retreat of the Antarctic Ice Sheet during the Last Interglaciation and implications for future change

N. R. Golledge[1], P. U. Clark[2,3], F. He[4], A. Dutton[5], C. S. M. Turney[6,7,8], C. J. Fogwill[6,9,10], T. R. Naish[1], R. H. Levy[1,11], R. M. Mckay[1], D. P. Lowry[11], N. A. N. Bertler[1,11], G. B. Dunbar[1], A. E. Carlson[12]

[1]Antarctic Research Centre, Victoria University of Wellington, Wellington 6140, New Zealand

[2]College of Earth, Ocean, and Atmospheric Sciences, Oregon State University, Corvallis, OR, USA

[3]School of Geography and Environmental Sciences, University of Ulster, Coleraine, UK

[4]Center for Climatic Research, Nelson Institute for Environmental Studies, University of Wisconsin-Madison, Madison, WI, USA

[5]Department of Geoscience, University of Wisconsin-Madison, Madison, WI, USA

[6]Earth and Sustainability Science Research Centre, School of Biological, Earth and Environmental Sciences, University of New South Wales, Kensington NSW 2033, Australia

[7]Australian Research Council Centre of Excellence in Australian Biodiversity and Heritage, School of Biological, Earth and Environmental Sciences, University of New South Wales, Kensington NSW 2033, Australia

[8]Chronos 14 Carbon-Cycle Facility, University of New South Wales, Sydney NSW 2052, Australia

[9]School of Geography, Geology and the Environment, Keele University, Staffordshire ST5 5BG, UK

[10]School of Water, Energy and the Environment, Cranfield University, College Road, Cranfield, MK43 0AL, UK

[11]GNS Science, Avalon, Lower Hutt 5011, New Zealand

[12]Oregon Glaciers Institute, Corvallis OR 97330, USA

Key Points:

- We present data-constrained simulations of the Antarctic Ice Sheet through the Last Interglaciation
- Our model predicts a maximum contribution to global mean sea level of 4 m at 126 ka BP
- Loss of much of the present-day West Antarctic Ice Sheet is already committed under current climate

Corresponding author: Nicholas R. Golledge, `nicholas.golledge@vuw.ac.nz`

Abstract

The Antarctic Ice Sheet (AIS) response to past warming consistent with the 1.5–2°C 'safe limit' of the United Nations Paris Agreement is currently not well known. Empirical evidence from the most recent comparable period, the Last Interglaciation, is sparse, and transient ice-sheet experiments are few and inconsistent. Here we present new, transient, GCM-forced ice-sheet simulations validated against proxy reconstructions. This is the first time such an evaluation has been attempted. Our empirically-constrained simulations indicate that the AIS contributed 4 m to global mean sea level by 126 ka BP, with ice lost primarily from the Amundsen, but not Ross or Weddell Sea, sectors. We resolve conflict between previous work and show that the AIS thinned in the Wilkes Subglacial Basin but did not retreat. We also find that the West Antarctic Ice Sheet may be predisposed to future collapse even in the absence of further environmental change, consistent with previous studies.

Plain Language Summary

Ice sheets can respond to climatic warming in complex ways, commonly only reaching a new state of balance many hundreds or even thousands of years after the initial change in climate has occurred. Here we investigate how the Antarctic Ice Sheet responded to a period of prolonged warmer-than-present climate that took place around 125000 years ago. At this time the global climate was only around 1 to 2°C above present, but geological records show that global sea level was at least 6 m, or maybe even as much as 9-11 m, higher than today. Our study shows that around 4 m of this could have come from Antarctica. Our model agrees well with geological evidence of enhanced ice discharge both close to the ice sheet and further afield. Applying this model to the future our experiments suggest that the West Antarctic Ice Sheet may already have been sufficiently destabilised to trigger a long-term sea level contribution of up to 4 m, even without further greenhouse gas emissions.

1 Introduction

Evidence of ice sheet changes during the last time when global mean sea level (GMSL) was above present is sparse. This period, the Last Interglaciation (LIG, 129–116 ka BP) was most likely characterised by a highstand in GMSL of 6–9 m (Masson-Delmotte et al., 2013; Dutton et al., 2015) or higher (Rohling et al., 2019), but global mean surface

temperatures (GMST) only slightly elevated (ca. +0.5–1.0°C) with respect to early industrial times (late 19th century) (Masson-Delmotte et al., 2013; Hoffman et al., 2017; Fischer et al., 2018; Turney, Jones, et al., 2020). GMST was amplified in the polar regions, with Arctic surface temperature anomalies of >3–11°C, substantially above the global mean (Landais et al., 2016; Yau et al., 2016; Fischer et al., 2018). Global mean ocean temperatures reached their maximum early in the LIG (129–127 ka BP) reaching 1.1±0.3°C above modern (approximately 2°C above early industrial; Shackleton et al., 2020). Around Antarctica, ocean temperatures reached their maxima ca. 129–127 ka BP in the Atlantic and Indian Ocean sectors, and ca. 125 ka BP in the Pacific sector (Chadwick et al., 2020). Warming of subsurface water relative to glacial maximum conditions exceeded sea surface warming during the LIG, and was most likely a consequence of a prolonged period of relatively weak Atlantic Meridional Overturning Circulation during the penultimate deglaciation (Marino et al., 2015; Clark et al., 2020; Turney, Fogwill, et al., 2020).

Thermal expansion of the ocean early in the LIG, peaking around 129 ka, accounts for up to 0.8 m sea-level-equivalent (SLE) change (Shackleton et al., 2020; Turney, Jones, et al., 2020) and although the timing of their retreat is not known, global glaciers could have contributed a maximum of 0.32 ± 0.08 m based on estimates of their current volume (Marzeion et al., 2020). The SLE contribution from the Greenland Ice Sheet (GrIS) is modelled to be anywhere from ca. 0.9 m (Clark et al., 2020) to ca. 5.1 m (Yau et al., 2016), with the majority of models and proxy-based reconstructions indicating likely mass loss in the 1–2 m SLE range (Colville et al., 2011; Dahl-Jensen et al., 2013; Calov et al., 2015; Goelzer et al., 2016; Bradley et al., 2018), most likely peaking or reaching peak contributions late in the LIG (post 125 ka).

The Antarctic Ice Sheet (AIS) has been less well studied, particularly in terms of ice sheet model (ISM) simulations that use ocean–atmosphere boundary conditions directly from general circulation models (GCM) or regional climate models (RCM). Whole-continent ISM reconstructions that have used environmental forcings directly from climate models without the ad hoc imposition of additional heat predict an AIS LIG contribution of 3–4.4 m (Goelzer et al., 2016; Clark et al., 2020). Whole continent as well as single catchment or limited area models have been used to investigate the sensitivity of key AIS drainage basins to both realistic and conceptual warming levels (Mengel & Levermann, 2014; Feldmann & Levermann, 2015; Golledge et al., 2017; Sutter et al.,

2020) but the scarcity of near-field empirical evidence with which to constrain ISM simulations prevents a critical evaluation of either the AIS contribution to LIG GMSL or the robustness of the models themselves.

Proxies that enable model–data comparison include stable isotope records from ice cores, which allow changes in surface temperatures and / or changes in surface elevation to be approximated if assumptions are made regarding past ice flow (Goursaud et al., 2020). Ice core studies can be used with climate model simulations to gauge whether changes in ice sheet geometry may have altered climatic conditions at a core site during periods of the past, such as the LIG (Steig et al., 2015). In addition to isotopic evidence of AIS change during the LIG there also exist a horizontal ice core record from the Patriot Hills (Horseshoe Valley, West Antarctica) (Turney, Fogwill, et al., 2020) and marine sediment records from offshore the Wilkes Subglacial Basin (WSB, East Antarctica) (Wilson et al., 2018) and the western Antarctic Peninsula (Carlson et al., 2021). The Patriot Hills blue ice record (Turney, Fogwill, et al., 2020) incorporates volcanic glass geochemically correlated with tephra in the Dome Fuji ice core, dated to 130.7 ± 1.8 ka BP (AICC2012 timescale; Hillenbrand et al., 2008), abruptly truncated by a hiatus in ice accumulation until ca. 80 ka BP. This hiatus is interpreted as evidence of dynamic thinning of this sector of the ice sheet during, and following, the LIG (Turney, Fogwill, et al., 2020). The marine sediment core offshore the WSB at U1361A reveals a clear signal of increased iceberg rafted debris (IBRD) over the site during the LIG, which together with provenance indicators from muds eroded off the continental margin suggests either a retreat of the ice margin in the WSB, or an increase in basal erosion and sediment transport from this area (Wilson et al., 2018). A second marine core, ODP 1096 (Fig. 1c), records only sediment sourced from the Antarctic Peninsula during the LIG but deposition of WAIS-derived sediment from 116 ka, suggesting perhaps that WAIS had retreated during the interglaciation and subsequently readvanced (Carlson et al., 2021).

No whole-continent AIS simulations have yet been explicitly assessed in terms of their agreement with the suite of proxy indicators of Antarctic ice-sheet changes described above. In this paper we therefore 1) present new ISM simulations for the period 140–116 ka BP, and 2) compare modelled changes with those inferred from ice-proximal and ice-distal proxy reconstructions described above.

2 Methods

We use the Parallel Ice Sheet Model (PISM; Bueler & Brown, 2009; Winkelmann et al., 2010), a fixed-grid thermodynamic ice sheet model that uses a hybrid stress balance combining shallow approximations of the flow equations for grounded and floating ice. PISM incoporates a 1-dimensional elastic lithosphere – relaxing asthenosphere solid earth deformation model based on the fast Fourier transform solution of Lingle and Clark (1985); Bueler et al. (2007), allowing us to capture the multi-millenial effects of ice loading on bedrock elevation. To ensure comparability of results with previous work, our simulations use the exact same parameterisations employed in Clark et al. (2020) except for modifications to mantle viscosity and bed elevation, as described in detail below. The optimal parameter set (Table S1) was chosen based on how well it allowed last glacial maximum and present day extents to be captured. Using a manual tuning procedure we explored the sensitivity of the model to changes in flow enhancement factors, basal substrate rheology and sliding parameters, different grounding line schemes, and calving approximations. We ran 103 transiently-forced simulations of 40–50 kyr duration each. The time evolution of grounded ice volume for these ensemble members is shown in Figure S1.

We implement the model at 20 km horizontal resolution and make use of the native subgrid grounding-line scheme to improve the sensitivity of this coarse grid simulation to oceanic forcing. Using spatially explicit, time varying, oceanic and atmospheric anomalies (compared to present day) from the National Center for Atmospheric Research Community Climate System Model version 3 (NCAR CCSM3; Clark et al., 2020) we run duplicate simulations for Termination 1 (T1; 20–0 ka BP) and Termination 2 (T2; 140–116 ka BP). We follow the exact same procedure as in Clark et al. (2020) and use simulations of the last glacial termination (T1) to ensure that our model can reproduce the extended glacial maximum configuration and present-day ice extent. Simulations for the penultimate glacial termination (T2) and Last Interglaciation are then run with the climate forcing (ocean temperature and salinity, air temperature, precipitation, global mean sea level) from CCSM3. A novel component of the new study presented here is that we also extend our T1 simulation for an additional 4 kyr, holding present-day (1979–2010) basal melt rates (Bernales et al., 2017) and atmospheric forcing (Golledge et al., 2019) fixed, in order to investigate the future dynamic (not climate-forced) response of the AIS.

Slow build-up of ice over the approximately 100 ka prior to both of the last two glacial terminations would have led to a bedrock elevation that was in equilibrium with the increased glacial maximum ice load above. To ensure that our simulations accurately reproduce this state before the start of the transient deglacial simulations we precede each of these simulations with a 20 kyr period during which a constant 'glacial maximum' climate field is applied. The conditions imposed during this phase are taken as the glacial maxima represented in the CCSM3 simulations at 140 ka and 20 ka BP for T2 and T1 respectively. Compared to Clark et al. (2020) our new simulations use an upper mantle viscosity value that is increased from 1.0×10^{19} Pa s to 1.3×10^{20} Pa s, as well as a topographic elevation correction to account for the effect of dynamic topography (Austermann et al., 2015) (Fig. S2). These modifications are implemented in an attempt to determine whether a better fit to the timing of AIS changes interpreted from the two key Antarctic glaciological and geological records described above (Wilson et al., 2018; Turney, Fogwill, et al., 2020) could be produced, compared to that in our original simulations (Clark et al., 2020). The dynamic topography correction accounts for at most an approximately 10 m lower bed in the Wilkes Subglacial Basin region (Fig. S2), whereas the changes to mantle rheology are more significant. We justify our imposed modification on the following grounds. In PISM v0.7.1 the 1-dimensional Earth deformation model uses a single upper mantle viscosity value for the whole domain. Our previous choice of 1.0×10^{19} Pa s is representative of inferences for West Antarctica from a range of studies (Table S2). However, considerable uncertainty exists, both in terms of vertical and horizontal heterogeneity, and values at or above 1×10^{20} Pa s have also been reported for West Antarctica and the Antarctic Peninsula (Wolstencroft et al., 2015; Bradley et al., 2015; Nield et al., 2016; Samrat et al., 2020; E. Ivins et al., 2021; Pan et al., 2021). Thus whilst West Antarctic upper mantle viscosity is considered to be low by Antarctic standards, our modified value is within the range of current estimates. Other published LIG ice sheet simulations (Goelzer et al., 2016; DeConto & Pollard, 2016) have both used a radially-symmetric 1-dimensional isostatic scheme from Huybrechts and de Wolde (1999), but that scheme 'produces results close to those from a full visco-elastic treatment with mantle viscosities in the range 0.5-1.0 $\times 10^{21}$ Pa s' (Huybrechts, 2002, p205), essentially 4 to 8 times stiffer than our parameterisation. In our simulations, iterative experimentation showed that only a narrow range of mantle viscosity values exists that allow present-day ground-

ing lines to be matched whilst also yielding above-present LIG mass loss (Figs. S3, S4) inferred from other studies (Fig. 1b; Kopp et al., 2009).

3 Results

Figure 1 illustrates the AIS response in terms of sea-level-equivalent mass loss to deglacial environmental forcings for (a) T1 and (b) T2. Sea-level-equivalent is calculated as the domain-integrated ice thickness above flotation compared to our modelled present-day geometry. Our frame-by-frame calculation captures temporal changes both in bedrock elevation and in ice thickness. Based on this approach, mass loss above present is first achieved shortly after 129 ka, peaking at 126 ka with a sea level contribution of 4.03 m. This ice volume minimum is maintained only briefly followed by a slow regrowth of the ice sheet and lowering of sea level to 118 ka, followed by renewed mass loss that continues to the end of the simulation at 116 ka. Both the timing and magnitude of peak modelled AIS mass loss are consistent with probabilistic estimates (Kopp et al., 2009) of the Southern Hemisphere sea-level contribution during this period (Fig. 1b, grey line and shading) but our modelled sea level contribution starts to exceed present-day sea level around 2000 years earlier than the Kopp et al. (2009) median. Comparison of isotopic changes in the Mt Moulton ice core (Steig et al., 2015) with climate model simulations have been used to infer little or no mass loss (relative to present) from the WAIS prior to 128 ka BP and maximum WAIS retreat by 126 ka (Holloway et al., 2016), which our simulation is also largely consistent with. The AIS contribution to LIG GMSL in our simulation is spatially heterogenous but comes primarily from the Thwaites and Pine Island Glacier catchments of the WAIS (Fig. 1c). As a consequence of CCSM3-simulated cooler-than-present subsurface ocean temperatures in the Ross and Weddell seas (Fig. S5), both the Ross and Filchner-Ronne ice shelves remain intact. In East Antarctica our modelled LIG grounded ice extent closely resembles its present-day configuration, with no substantial grounding line retreat apparent in either the WSB, the Aurora Basin, or the Recovery catchment (Fig. 1c).

Closer investigation of the Amundsen Sea Embayment reveals that the retreating grounding line in this area migrates inland of its present-day position shortly after 130 ka BP and progressively evacuates the interior of WAIS over the subsequent 3–4 kyr (Fig. 2). This is consistent with the timing of WAIS retreat inferred from marine sediments at ODP 1096 (Carlson et al., 2021), if uncertainties associated with the bounding tephra

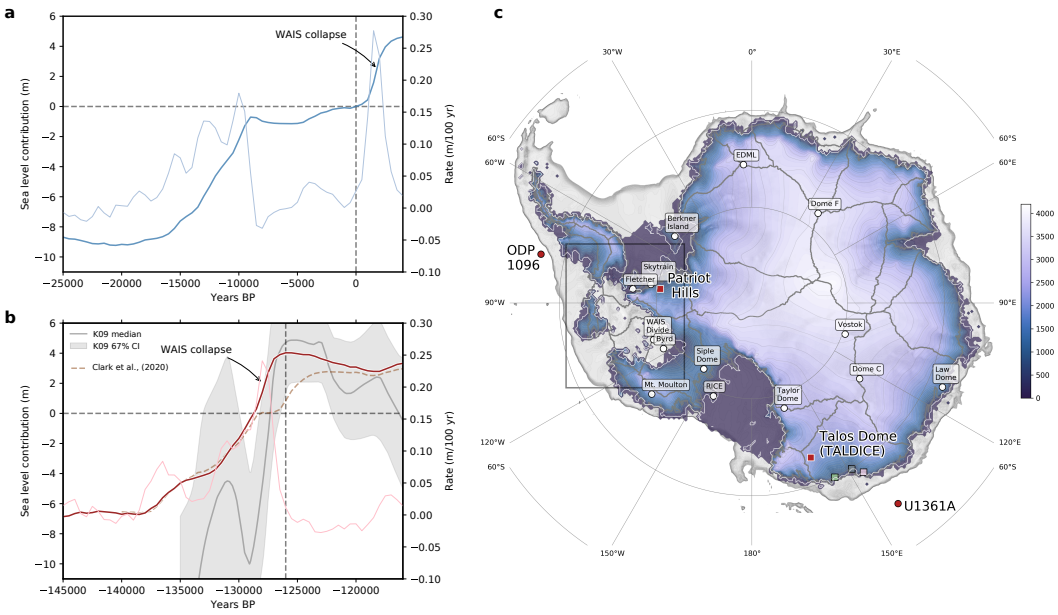

Figure 1. Simulated mass loss from the Antarctic Ice Sheet (bold lines) during a) the last and b) the penultimate glacial terminations. Rates-of-change shown with thinner lines in each panel. Modelled LIG sea-level-equivalent mass loss from Clark et al. (2020) shown with dashed brown line in b) for comparison to the new simulation. Median and 67% confidence interval of a probabilistic reconstruction of the Southern Hemisphere contribution to global mean sea level shown with grey line and shading (Kopp et al., 2009). c) Surface elevation (metres) of the modelled Antarctic Ice Sheet at 126 ka BP when peak LIG mass loss is reached. Patriot Hills blue ice area, Talos Dome ice core site, ODP1096 and U1361A marine sediment core locations and the three sites (coloured boxes) investigated in Figure 4 also shown. Labeled white squares identify other ice core locations for which predictions of ice sheet change are presented in Figure S6. Grey lines show present-day boundaries of grounded ice catchments (Zwally et al., 2012). Black rectangle denotes area shown in Figure 2.

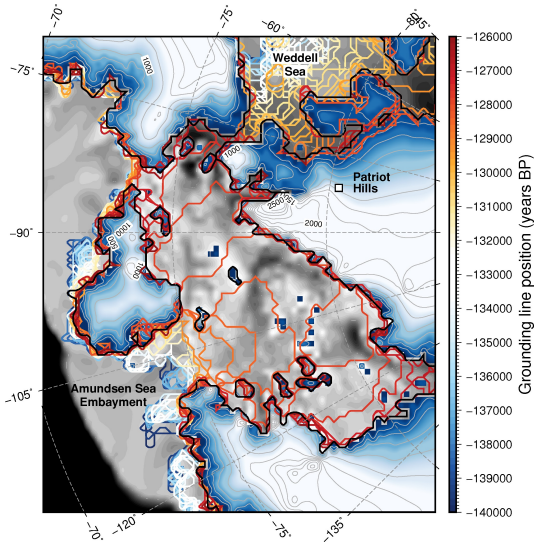

Figure 2. Grounding line retreat in the Amundsen Sea Embayment from 140–126 ka BP. Retreat proceeds rapidly into the interior of WAIS once the pinning point near the present-day grounding line is lost. Grounding line retreat in the Weddell Sea is slower, but takes place earlier. Blue-to-white shading and labelled contour lines show ice elevation; colored lines denote the modelled age of the grounding line position. Location of Patriot Hills ice core record (Turney, Fogwill, et al., 2020) also shown.

age (130.7 ± 1.8 ka; Hillenbrand et al., 2008) are considered. Grounded ice in the Weddell Sea embayment appears to retreat to close to its present-day extent in the millennia just before and just after 130 ka, and then stabilises. Comparison of modelled grounding-line positions in the Weddell and Amundsen Sea sectors highlights the far more rapid retreat in the latter, consistent with previous interpretations of LIG marine ice sheet instability in this sector (Clark et al., 2020). The more-rapid retreat we simulate than modelled previously (Fig. 1b) arises from our stiffer mantle parameterisation ('Methods', above), leading to slower isostatic rebound that gives rise to deeper water during WAIS retreat.

To gauge the degree of fit between our simulation and two empirical studies that report isotopic evidence of changes in the AIS during the LIG, we first consider the isotope record recovered from the Blue Ice Area (BIA) of Horseshoe Valley, in the Patriot Hills of West Antarctica (278.65° E, 80.3° S, Figs. 1c & 2; Turney, Fogwill, et al., 2020). Although our 20 km resolution simulation is unable to simulate the detailed pattern of ice flow in the 30 km-wide Horseshoe Valley, our previous work has shown that behaviour of this glacier is controlled to a large degree by activity of the Institute Ice Stream and

regional ice flow patterns spanning length scales on the order of hundreds of kilometers (Fogwill et al., 2014; Winter et al., 2016; Turney, Fogwill, et al., 2020). The BIA horizontal core preserves tephra that is geochemically correlated to the Dome Fuji ice core, thereby stratigraphically linking East and West Antarctic ice sheets. Stratigrapically above this horizon is a disconformity, representing an interval from 130 ka to 80 ka when ice layers are absent. These missing layers could imply either a hiatus in accumulation, or post-depositional loss. Our simulation predicts a 5000-year long episode of regional-scale ice thinning that coincides with the timing of tephra deposition and the beginning of the isotopic hiatus (Fig. 3a). If this thinning had been driven by surface ablation (wind-induced sublimation) the tephra would not be preserved in situ. Conversely, if thinning were instead primarily the result of melting at the bed rather than at the surface, then the younger ice overlying the tephra should still be preserved, yet this is not the case.

In our simulation the onset of thinning appears to be a response to a steady increase in surface velocity that started around 132.5 ka (Fig. 3b, red line). This date corresponds to the timing of southward retreat of the ice sheet grounding line in the Weddell Sea (Fig. 2) that triggered regional uplift at the BIA site from ca. 131 ka BP (Fig. 3b, blue line). Combined with collapse of the ASE glaciers from 129 ka (Fig. 2) the reduction in regional ice loading led to accelerated bedrock rebound and promoted faster basal sliding due to the increase in topographic gradient (Fig. 3b, black line).

Since modelled surface velocities are an order of magnitude greater than the rate of basal sliding, flow must have occurred primarily by shear (internal deformation). Under this kind of flow regime, the increasing surface slope and surface velocity driven by Weddell Sea grounding line retreat and bedrock uplift would have led to faster flow and extensional thinning near the surface compared to in deeper ice layers. Thinning rates increased gradually from 132.5 ka BP reaching a maximum of around 0.5 m/year by ca. 128.5 ka BP (Fig. 3a). Snow layers accumulating during this time would have thus become increasingly thinned, relative to older layers beneath, as they flowed from their original location to the BIA sample site downstream. In this scenario, the apparent hiatus actually may represent a period of enhanced layer thinning that allowed stratigraphically separated isochrones to eventually intersect (Fig. 3c). Although our simulations do not extend to 80 ka BP, we surmise that thinning halted at 80 ka because of renewed isostatic loading due to ASE regrowth, and/or because of readvance of Weddell Sea grounding lines as the climate cooled. We caution, however, that our conceptual interpretation

of this apparent hiatus is just one of many possibilities, and a more detailed study using a more highly-vertically-resolved ice sheet model could be used to test this. To put the Patriot Hills record in context, we extracted modelled changes in ice sheet thickness and elevation at 15 other west and east Antarctic ice core sites (Fig. 1c; Fig. S6). Whilst the East Antarctic locations (Dome C, Vostok, Dome F, EDML, Law Dome, TALDICE, Taylor Dome) and Berkner Island and Mt Moulton sites in West Antarctica exhibit only minor modelled deviations from present, more substantial changes (hundreds of metres) are seen at RICE, Siple Dome, Patriot Hills, Skytrain, and Fletcher Promontory. Our model predicts complete ice sheet loss at the WAIS Divide and Byrd ice core locations in West Antarctica, as a consequence of westward ice divide and grounding line migration (Fig. 1c). Furthermore, our model also allows us to predict where surface elevation changes may be explained partially or wholly by bedrock uplift associated with regional ice loss, which could help more accurately interpret isotopic changes from ice core records (Fig. S6).

Many studies have considered the possibility that the WSB in East Antarctica could have collapsed during warmer periods of the past (Cook et al., 2013; Mengel & Levermann, 2014; Patterson et al., 2014; Golledge et al., 2017; Bertram et al., 2018), but to date there is no evidence that unequivocally proves ice loss from this sector of the ice sheet. In lieu of glaciological evidence we use geological records of sediment provenance changes from marine sediment core U1361A at 143.89°E, 64.41°S (Wilson et al., 2018). This archive preserves IBRD, as well as laminated clays whose barium/aluminium ratio indicates changes in sea ice extent and biological productivity. Co-variance of these markers with evidence of inland glacial erosion from geochemical provenance studies (Nd isotopes) has been used to suggest that reduced sea ice during Pleistocene interglacials was coincident with increased sediment erosion from the WSB, perhaps because of retreat of the ice margin (Wilson et al., 2018, Fig. 4d). Inland terrestrial geochemical records, however, suggest that the WSB has been ice-filled since c. 400 ka BP (Blackburn et al., 2020), and hence if it did contribute to higher-than-present LIG GMSL, the contribution may have been relatively minor. Recent high-resolution ice sheet modelling as well as general circulation model (GCM) experiments support this latter interpretation, showing that the isotopic record preserved in the Talos Dome ice core is inconsistent with the surface lowering of that area that would have occurred had the WSB deglaciated sub-

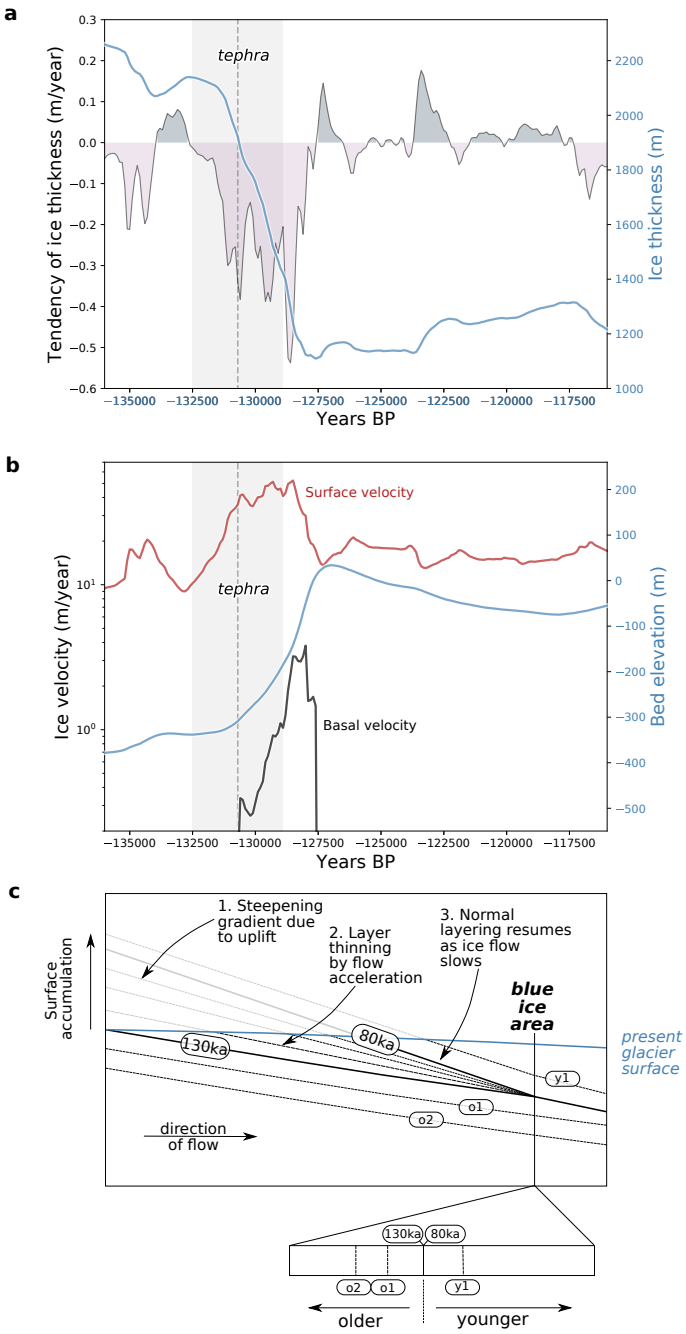

Figure 3. a) Modelled ice thickness and its rate of change, and b) bed elevation, and surface and basal velocity at the Patriot Hills blue ice area through the period 132–116 ka BP. Timing of tephra horizon marking the beginning of the hiatus in the core (Turney, Fogwill, et al., 2020) also shown (dotted line), including age uncertainty (grey shading). c) Schematic explanation of the mechanism leading to the c. 130–80 ka BP hiatus in the Patriot Hills ice core record. Steepening of the ice surface due to bedrock uplift and grounding-line retreat lead to enhancing thinning as ice is advected more quickly downglacier, eventually allowing time-separated ice layers (isochrones) to converge.

stantially (Sutter et al., 2020; Goursaud et al., 2020). Sutter et al. (2020) conclude that during the LIG the WSB could have contributed only up to ca. 0.8 m SLE.

Here we unify these studies. Figure 4a shows our modelled ice surface elevation over the WSB during the LIG at 126 ka BP when modelled Antarctic ice loss peaked. Figure 4c shows modelled surface elevation change at Talos Dome from 132 – 116 ka (blue line), and indicates changes of approximately 100 m over 10000 years, consistent with the TALDICE reconstruction (Sutter et al., 2020). We also track changes in ice elevation and basal ice velocity in the key outlet glaciers of this region: Cook, Ninnis, and Mertz (Fig. 4e,f). In contrast to the large-scale retreat in the ASE shown in Figure 2, our model predicts a stable margin in the WSB sector. Based on previous experimentation in which we explored the environmental sensitivity of each Antarctic catchment in detail (Golledge et al., 2017) we conclude that the WSB remained stable during the LIG due to insufficient atmospheric warming that would have been needed to thin the ice sheet enough to render it vulnerable to ocean thermal forcing and grounding line retreat. Even in the absence of grounding-line retreat in this area, however, we simulate thinning of up to 500 m in the trunk of the Ninnis Glacier, coupled with an abrupt increase in sliding velocity from approximately 150 m/year to 450 m/year. Because these accelerations are localised, however, the sea-level equivalent volume of this catchment is only 0.05 m less than in our modelled present-day geometry. Our modelled ice dynamic changes are coeval with the IBRD, Ba/Al, and Nd-based interpretations of ice sheet change shown in Figure 4d,e,f. Since sliding velocity controls basal erosion and subglacial sediment transport (Pollard & DeConto, 2003; Herman et al., 2015), our modelled ice flow acceleration can plausibly explain the increased inland basal erosion inferred from marine sediment core U1361A (Wilson et al., 2018).

4 Implications for future change

Our new simulation, using a stiffer mantle compared to our previous experiments (Clark et al., 2020), produces a simulated LIG AIS evolution that is temporally and spatially consistent with Antarctic marine sediment records, glaciological records of ice thickness change, and with probabilistic assessments of global mean sea level. Using this empirically-constrained model we are also able to make inferences regarding future AIS evolution. In particular, one notable feature of our T1 tuning experiment (Fig. 1a) is that after a period of relative stability during the Holocene (approximately the last 10,000 years),

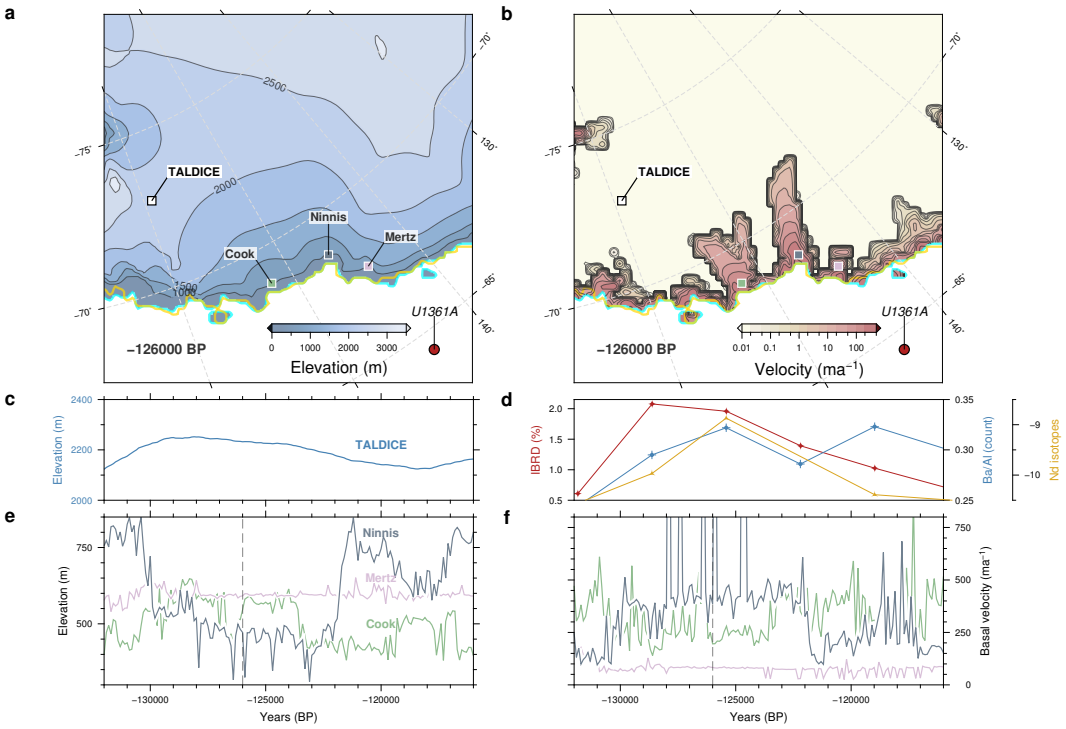

Figure 4. Ice thickness and basal ice velocity changes in the Wilkes Subglacial Basin during the period 132–116ka BP. a) Modelled ice elevation and b) basal ice velocity at 126 ka BP showing location of the three main outlet glaciers in this region. Location of the Talos Dome ice core site (TALDICE) and marine sediment core U1361A also shown. Gold and cyan lines shows present-day and 126 ka BP grounding-line positions respectively. c) Timeseries of modelled ice elevation changes and d) sediment proxies from U1361A compared to e) modelled elevation and f) basal velocity changes at the three glacier trunks shown in a). The model predicts substantial thinning and acceleration of Ninnis Glacier coincident with increased sediment flux to U1361A, yet without impact on ice thickness at Talos Dome. Vertical dotted lines identify the timeslice shown in panels a) and b)

our model predicts renewed, and rapid, AIS mass loss beginning c. 1500 years after present day. The trajectory of ice loss over the period 1500-4000 years into the future is similar to the pattern of loss taking place during the early millennia of the LIG (Fig. 1b), reflecting MISI-forced collapse of the ASE sector of WAIS. Given that no additional environmental forcing is applied during this period (from year 0 into the future), the lagged response is most likely a consequence of our basal melt parameterisation, which is optimised to closely reproduce present-day (1979–2010) melt rates (Bernales et al., 2017; Golledge et al., 2019). The implication therefore is that ocean warming to-date is already sufficient to trigger millennial-scale collapse of part of West Antarctica, as has been found previously (Joughin et al., 2014; Arthern & Williams, 2017; Golledge et al., 2019; Garbe et al., 2020).

Acknowledgments

Ice sheet model outputs shown in this paper are available at the Open Science Framework (https://doi.org/10.17605/OSF.IO/GZB3H). Climate model outputs used are available at https://doi.org/10.17605/OSF.IO/FX7WK. NRG acknowledges funding from Royal Society of New Zealand contract VUW-1501. Simulations on which this work is based were funded by US National Science Foundation (NSF) through grant numbers AGS-1503032 (to PUC and AEC), AGS-1502990 (to FH), 1559040 (to AD) and OPP-1443437 (to AEC). FH gratefully acknowledges the NOAA Climate and Global Change Postdoctoral Fellowship programme, administered by the University Corporation for Atmospheric Research. High-performance computing support from Yellowstone (http://n2t.net/ark:/85065/d7wd3xhc) and Cheyenne (http://www.doi.org/10.5065/D6RX99HX) was provided by NCARs Computational and Information Systems Laboratory, sponsored by the NSF. This research used resources of the Oak Ridge Leadership Computing Facility at the Oak Ridge National Laboratory, which is supported by the Office of Science of the US Department of Energy under contract number DE-AC05-00OR22725. AD gratefully acknowledges the U.S. Fulbright Scholar Program. CSMT and CJF acknowledge support from the Australian Research Council (ARC), including Linkage Project (LP120200724)and Discovery Project DP210103621, supported by Antarctic Logistics and Expeditions. NRG, TRN, RHL, RMM, DPL, NANB and GBD acknowledge support from Ministry for Business, Innovation and Employment contracts RTUV1705 ('NZSeaRise') and ANTA1801 ('Antarc-

tic Science Platform'). PISM is supported by NASA grant numbers NNX13AM16G and NNX13AK27G. The authors declare no financial conflicts of interest.

References

Arthern, R. J., & Williams, C. R. (2017). The sensitivity of West Antarctica to the submarine melting feedback. *Geophysical Research Letters*, *44*(5), 2352–2359.

Austermann, J., Pollard, D., Mitrovica, J. X., Moucha, R., Forte, A. M., DeConto, R. M., ... Raymo, M. E. (2015). The impact of dynamic topography change on Antarctic ice sheet stability during the mid-Pliocene warm period. *Geology*, *43*(10), 927–930.

Barletta, V. R., Bevis, M., Smith, B. E., Wilson, T., Brown, A., Bordoni, A., ... others (2018). Observed rapid bedrock uplift in Amundsen Sea Embayment promotes ice-sheet stability. *Science*, *360*(6395), 1335–1339.

Bernales, J., Rogozhina, I., & Thomas, M. (2017). Melting and freezing under Antarctic ice shelves from a combination of ice-sheet modelling and observations. *Journal of Glaciology*, *63*, 731-744.

Bertram, R. A., Wilson, D. J., van de Flierdt, T., McKay, R. M., Patterson, M. O., Jimenez-Espejo, F. J., ... Riesselman, C. R. (2018). Pliocene deglacial event timelines and the biogeochemical response offshore Wilkes Subglacial Basin, East Antarctica. *Earth and Planetary Science Letters*, *494*, 109–116.

Blackburn, T., Edwards, G. H., Tulaczyk, S., Scudder, M., Piccione, G., Hallet, B., ... Babbe, J. T. (2020). Ice retreat in Wilkes Basin of East Antarctica during a warm interglacial. *Nature*, *583*, 554-559.

Bradley, S. L., Hindmarsh, R. C. A., Whitehouse, P. L., Bentley, M. J., & King, M. A. (2015). Low post-glacial rebound rates in the weddell sea due to late holocene ice-sheet readvance. *Earth and Planetary Science Letters*, *413*, 79–89.

Bradley, S. L., Reerink, T. J., Van De Wal, R. S., & Helsen, M. M. (2018). Simulation of the Greenland Ice Sheet over two glacial-interglacial cycles: investigating a sub-ice-shelf melt parameterization and relative sea level forcing in an ice-sheet-ice-shelf model. *Climate of the Past*, *14*(5), 619–635.

Bueler, E., & Brown, J. (2009). Shallow shelf approximation as a "sliding law" in a thermomechanically coupled ice sheet model. *Journal of Geophysical Research*,

114, F03008.

Bueler, E., Lingle, C., & Brown, J. (2007). Fast computation of a viscoelastic deformable Earth model for ice-sheet simulations. *Annals of Glaciology*, *46*, 97-105.

Buizert, C., Gkinis, V., Severinghaus, J. P., He, F., Lecavalier, B. S., Kindler, P., ... others (2014). Greenland temperature response to climate forcing during the last deglaciation. *Science*, *345*(6201), 1177–1180.

Calov, R., Robinson, A., Perrette, M., & Ganopolski, A. (2015). Simulating the Greenland ice sheet under present-day and palaeo constraints including a new discharge parameterization. *The Cryosphere*, *9*, 179–196.

Carlson, A. E., Beard, B. L., Hatfield, R. G., & Laffin, M. (2021). Absence of West Antarctic-sourced silt at ODP Site 1096 in the Bellingshausen Sea during the last interglaciation: Support for West Antarctic ice-sheet deglaciation. *Quaternary Science Reviews*, *261*, 106939.

Chadwick, M., Allen, C., Sime, L., & Hillenbrand, C.-D. (2020). Analysing the timing of peak warming and minimum winter sea-ice extent in the Southern Ocean during MIS 5e. *Quaternary Science Reviews*, *229*, 106134.

Clark, P. U., He, F., Golledge, N. R., Mitrovica, J. X., Dutton, A., Hoffman, J. S., & Dendy, S. (2020). Oceanic forcing of penultimate deglacial and last interglacial sea-level rise. *Nature*, *577*, 660-664.

Colville, E. J., Carlson, A. E., Beard, B. L., Hatfield, R. G., Stoner, J. S., Reyes, A. V., & Ullman, D. J. (2011). Sr-Nd-Pb Isotope Evidence for Ice-Sheet Presence on Southern Greenland During the Last Interglacial. *Science*, *333*, 620-623.

Cook, C. P., van de Flierdt, T., Williams, T., Hemming, S. R., Iwai, M., Kobayashi, M., ... others (2013). Dynamic behaviour of the East Antarctic ice sheet during Pliocene warmth. *Nature Geoscience*, *6*(9), 765–769.

Dahl-Jensen, D., Albert, M., Aldahan, A., Azuma, N., Balslev-Clausen, D., Baumgartner, M., ... others (2013). Eemian interglacial reconstructed from a Greenland folded ice core. *Nature*, *493*(7433), 489.

DeConto, R., & Pollard, D. (2016). Contribution of Antarctica to past and future sea-level rise. *Nature*, *531*, 591-597.

Dutton, A., Carlson, A., Long, A., Milne, G., Clark, P., DeConto, R., ... Raymo,

M. (2015). Sea-level rise due to polar ice-sheet mass loss during past warm periods. *Science*, *349*, aaa4019.

Feldmann, J., & Levermann, A. (2015). Interaction of marine ice-sheet instabilities in two drainage basins: simple scaling of geometry and transition time. *The Cryosphere*, *9*, 631–645.

Fischer, H., Meissner, K. J., Mix, A. C., Abram, N. J., Austermann, J., Brovkin, V., ... others (2018). Palaeoclimate constraints on the impact of 2°c anthropogenic warming and beyond. *Nature Geoscience*, *11*(7), 474.

Fogwill, C., Turney, C., Golledge, N., Rood, D., Hippe, K., Wacker, L., ... Jones, R. (2014). Drivers of abrupt Holocene shifts in West Antarctic ice stream direction determined from combined ice sheet modelling and geologic signatures. *Antarctic Science*, *26*(6), 674–686.

Garbe, J., Albrecht, T., Levermann, A., Donges, J. F., & Winkelmann, R. (2020). The hysteresis of the Antarctic ice sheet. *Nature*, *585*(7826), 538–544.

Goelzer, H., Huybrechts, P., Loutre, M.-F., & Fichefet, T. (2016). Last Interglacial climate and sea-level evolution from a coupled ice sheet–climate model. *Climate of the Past*, *12*(12), 2195–2213.

Golledge, N., Menviel, L., Carter, L., Fogwill, C., England, M., Cortese, G., & Levy, R. (2014). Antarctic contribution to meltwater pulse 1A from reduced Southern Ocean overturning. *Nature Communications*, *(5)*, 1-10. doi: doi:10.1038/ncomms6107

Golledge, N., Thomas, Z., Levy, R., Gasson, E., Naish, T., McKay, R., ... Fogwill, C. (2017). Antarctic climate and ice sheet configuration during a peak-warmth Early Pliocene interglacial. *Climate of the Past*, *13*, 959975.

Golledge, N. R., Keller, E. D., Gomez, N., Naughten, K. A., Bernales, J., Trusel, L. D., & Edwards, T. L. (2019). Global environmental consequences of twenty-first-century ice-sheet melt. *Nature*, *566*, 65-72.

Golledge, N. R., Levy, R. H., McKay, R. M., & Naish, T. R. (2017). East Antarctic ice sheet most vulnerable to Weddell Sea warming. *Geophysical Research Letters*, *44*, 2343–2351.

Goursaud, S., Holloway, M., Sime, L., Wolff, E., Valdes, P., Steig, E. J., & Pauling, A. (2020). Antarctic Ice Sheet elevation impacts on water isotope records during the Last Interglacial. *Geophysical Research Letters*, e2020GL091412.

He, F., Shakun, J. D., Clark, P. U., Carlson, A. E., Liu, Z., Otto-Bliesner, B. L., & Kutzbach, J. E. (2013). Northern Hemisphere forcing of Southern Hemisphere climate during the last deglaciation. *Nature*, *494*(7435), 81–85.

Herman, F., Beyssac, O., Brughelli, M., Lane, S. N., Leprince, S., Adatte, T., ... Cox, S. C. (2015). Erosion by an Alpine glacier. *Science*, *350*(6257), 193–195.

Hillenbrand, C.-D., Moreton, S., Caburlotto, A., Pudsey, C., Lucchi, R., Smellie, J., ... Larter, R. (2008). Volcanic time-markers for Marine Isotopic Stages 6 and 5 in Southern Ocean sediments and Antarctic ice cores: implications for tephra correlations between palaeoclimatic records. *Quaternary Science Reviews*, *27*(5-6), 518–540.

Hoffman, J. S., Clark, P. U., Parnell, A. C., & He, F. (2017). Regional and global sea-surface temperatures during the last interglaciation. *Science*, *355*(6322), 276–279.

Holloway, M. D., Sime, L. C., Singarayer, J. S., Tindall, J. C., Bunch, P., & Valdes, P. J. (2016). Antarctic last interglacial isotope peak in response to sea ice retreat not ice-sheet collapse. *Nature Communications*, *7*(1), 1–9.

Huybrechts, P. (2002). Sea-level changes at the LGM from ice-dynamic reconstructions of the Greenland and Antarctic ice sheets during the glacial cycles. *Quaternary Science Reviews*, *21*(1-3), 203–231.

Huybrechts, P., & de Wolde, J. (1999). The dynamic response of the Greenland and Antarctic ice sheets to multiple-century climatic warming. *Journal of Climate*, *12*(8), 2169–2188.

Huybrechts, P., & De Wolde, J. (1999). The dynamic response of the greenland and antarctic ice sheets to multiple-century climatic warming. *Journal of Climate*, *12*(8 PART 1), 2169–2188.

Ivins, E., van der Wal, W., Wiens, D., Lloyd, A., & Caron, L. (2021). *Antarctic mantle rheology*. London, UK: Geological Society of London.

Ivins, E. R., Watkins, M. M., Yuan, D.-N., Dietrich, R., Casassa, G., & Rülke, A. (2011). On-land ice loss and glacial isostatic adjustment at the Drake Passage: 2003–2009. *Journal of Geophysical Research: Solid Earth*, *116*(B2).

Joughin, I., Smith, B. E., & Medley, B. (2014). Marine Ice Sheet Collapse Potentially Under Way for the Thwaites Glacier Basin, West Antarctica. *Science*, *344*, 735-738.

Kopp, R. E., Simons, F. J., Mitrovica, J. X., Maloof, A. C., & Oppenheimer, M. (2009, December). Probabilistic assessment of sea level during the last interglacial stage. *Nature*, *462*(7275), 863–867. doi: 10.1038/nature08686

Landais, A., Masson-Delmotte, V., Capron, E., Langebroek, P. M., Bakker, P., Stone, E. J., ... others (2016). How warm was Greenland during the last interglacial period? *Climate of the Past*, *12*(9), 1933–1948.

Levitus, S., Antonov, J. I., Boyer, T. P., Baranova, O. K., Garcia, H. E., Locarnini, R. A., ... others (2012). World ocean heat content and thermosteric sea level change (0–2000 m), 1955–2010. *Geophysical Research Letters*, *39*(10).

Lingle, C., & Clark, J. (1985). A numerical model of interactions between a marine ice sheet and the solid earth: Application to a West Antarctic ice stream. *Journal of Geophysical Research*, *90*, 1100-1114.

Marcott, S. A., Clark, P. U., Padman, L., Klinkhammer, G. P., Springer, S. R., Liu, Z., ... Schmittner, A. (2011). Ice-shelf collapse from subsurface warming as a trigger for Heinrich events. *Proceedings of the National Academy of Sciences*, *108*, 13415-13419.

Marino, G., Rohling, E., Rodriguez-Sanz, L., Grant, K., Heslop, D., Roberts, A., ... Yu, J. (2015). Bipolar seesaw control on last interglacial sea level. *Nature*, *522*, 197-201.

Marzeion, B., Hock, R., Anderson, B., Bliss, A., Champollion, N., Fujita, K., ... others (2020). Partitioning the uncertainty of ensemble projections of global glacier mass change. *Earth's Future*, e2019EF001470.

Masson-Delmotte, V., Schulz, M., Abe-Ouchi, A., Beer, J., Ganopolski, A., González Rouco, J., ... Timmermann, A. (2013). Information from Paleoclimate Archives. In T. Stocker et al. (Eds.), *Climate Change 2013 : The Physical Science Basis. Contribution of Working Group I to the Fifth Assessment Report of the Intergovernmental Panel on Climate Change* (p. 383-464).

Mengel, M., & Levermann, A. (2014). Ice plug prevents irreversible discharge from East Antarctica. *Nature Climate Change*, *4*, 451–455.

Menviel, L., Timmermann, A., Timm, O. E., & Mouchet, A. (2010). Climate and biogeochemical response to a rapid melting of the West Antarctic Ice Sheet during interglacials and implications for future climate. *Paleoceanography*, *25*.

Naughten, K. A., Meisssner, K. J., Galton-Fenzi, B. K., England, M. H., Timmer-

mann, R., & Hellmer, H. H. (2018). Future Projections of Antarctic Ice Shelf Melting Based on CMIP5 Scenarios. *Journal of Climate*, *31*, 5243-5261.

Nield, G. A., Barletta, V. R., Bordoni, A., King, M. A., Whitehouse, P. L., Clarke, P. J., ... Berthier, E. (2014). Rapid bedrock uplift in the Antarctic Peninsula explained by viscoelastic response to recent ice unloading. *Earth and Planetary Science Letters*, *397*, 32–41.

Nield, G. A., Whitehouse, P. L., King, M. A., & Clarke, P. J. (2016). Glacial isostatic adjustment in response to changing Late Holocene behaviour of ice streams on the Siple Coast, West Antarctica. *Geophysical Supplements to the Monthly Notices of the Royal Astronomical Society*, *205*(1), 1–21.

Pan, L., Powell, E. M., Latychev, K., Mitrovica, J. X., Creveling, J. R., Gomez, N., ... Clark, P. U. (2021). Rapid postglacial rebound amplifies global sea level rise following West Antarctic Ice Sheet collapse. *Science Advances*, *eabf7787*, 1-9.

Patterson, M., McKay, R., Naish, T., Escutia, C., Jimenez-Espejo, F., Raymo, M., ... IODP Expedition 318 scientists (2014). Orbital forcing of the East Antarctic ice sheet during the Pliocene and Early Pleistocene. *Nature Geoscience*, *7*, 841–847.

Pollard, D., & DeConto, R. M. (2003). Antarctic ice and sediment flux in the Oligocene simulated by a climate-ice sheet-sediment model. *Palaeogeography, Palaeoclimatology, Palaeoecology*, *198*, 53–67.

Powell, E., Gomez, N., Hay, C., Latychev, K., & Mitrovica, J. (2020). Viscous effects in the solid Earth response to modern Antarctic ice mass flux: Implications for geodetic studies of WAIS stability in a warming world. *Journal of Climate*, *33*(2), 443–459.

Rohling, E. J., Hibbert, F. D., Grant, K. M., Galaasen, E. V., Irvalı, N., Kleiven, H. F., ... others (2019). Asynchronous Antarctic and Greenland ice-volume contributions to the last interglacial sea-level highstand. *Nature Communications*, *10*(1), 1–9.

Samrat, N. H., King, M. A., Watson, C., Hooper, A., Chen, X., Barletta, V. R., & Bordoni, A. (2020). Reduced ice mass loss and three-dimensional viscoelastic deformation in northern Antarctic Peninsula inferred from GPS. *Geophysical Journal International*, *222*(2), 1013–1022.

Shackleton, S., Baggenstos, D., Menking, J., Dyonisius, M., Bereiter, B., Bauska, T., ... others (2020). Global ocean heat content in the Last Interglacial. *Nature Geoscience*, *13*(1), 77–81.

Simms, A. R., Ivins, E. R., DeWitt, R., Kouremenos, P., & Simkins, L. M. (2012). Timing of the most recent Neoglacial advance and retreat in the South Shetland Islands, Antarctic Peninsula: insights from raised beaches and Holocene uplift rates. *Quaternary Science Reviews*, *47*, 41–55.

Steig, E. J., Huybers, K., Singh, H. A., Steiger, N. J., Ding, Q., Frierson, D. M., ... White, J. W. (2015). Influence of West Antarctic ice sheet collapse on Antarctic surface climate. *Geophysical Research Letters*, *42*(12), 4862–4868.

Sutter, J., Eisen, O., Werner, M., Grosfeld, K., Kleiner, T., & Fischer, H. (2020). Limited retreat of the Wilkes Basin ice sheet during the Last Interglacial. *Geophysical Research Letters*, *47*(13), e2020GL088131.

Sutter, J., Gierz, P., Grosfeld, K., Thoma, M., & Lohmann, G. (2016). Ocean temperature thresholds for last interglacial West Antarctic ice sheet collapse. *Geophysical Research Letters*, *43*(6), 2675–2682.

Turney, C., Fogwill, C., Golledge, N., McKay, N. P., van Sebille, E., Jones, R. T., ... others (2020). Early Last Interglacial ocean warming drove substantial ice mass loss from Antarctica. *Proceedings of the National Academy of Sciences*, *117*(8), 3996–4006.

Turney, C., Jones, R., McKay, N., Van Sebille, E., Thomas, Z., Hillenbrand, C.-D., & Fogwill, C. (2020). A global mean sea surface temperature dataset for the Last Interglacial (129–116 ka) and contribution of thermal expansion to sea level change. *Earth System Science Data*, *12*(4), 3341–3356.

Wilson, D. J., Bertram, R. A., Needham, E. F., van de Flierdt, T., Welsh, K. J., McKay, R. M., ... Escutia, C. (2018). Ice loss from the East Antarctic Ice Sheet during late Pleistocene interglacials. *Nature*, *561*(7723), 383–386.

Winkelmann, R., Martin, M. A., Haseloff, M., Albrecht, T., Bueler, E., Khroulev, C., & Levermann, A. (2010, August). The Potsdam Parallel Ice Sheet Model (PISM-PIK) - Part 1: Model description. *The Cryosphere*, *5*, 715–726.

Winter, K., Woodward, J., Dunning, S. A., Turney, C. S., Fogwill, C. J., Hein, A. S., ... others (2016). Assessing the continuity of the blue ice climate record at Patriot Hills, Horseshoe Valley, West Antarctica. *Geophysical Research Letters*,

43(5), 2019–2026.

Wolstencroft, M., King, M. A., Whitehouse, P. L., Bentley, M. J., Nield, G. A., King, E. C., ... others (2015). Uplift rates from a new high-density GPS network in Palmer Land indicate significant late Holocene ice loss in the south-western Weddell Sea. *Geophysical Journal International*, *203*(1), 737–754.

Yau, A. M., Bender, M. L., Robinson, A., & Brook, E. J. (2016). Reconstructing the last interglacial at Summit, Greenland: Insights from GISP2. *Proceedings of the National Academy of Sciences*, *113*(35), 9710–9715.

Zhao, C., King, M. A., Watson, C. S., Barletta, V. R., Bordoni, A., Dell, M., & Whitehouse, P. L. (2017). Rapid ice unloading in the Fleming Glacier region, southern Antarctic Peninsula, and its effect on bedrock uplift rates. *Earth and Planetary Science Letters*, *473*, 164–176.

Zwally, H. J., Giovinetto, M. B., Beckley, M. A., & Saba, J. L. (2012). Antarctic and Greenland Drainage Systems. *GSFC Cryospheric Sciences Laboratory*, http://icesat4.gsfc.nasa.gov/cryo_data/ant_grn_drainage_systems.php.

Supporting Information for "Retreat of the Antarctic Ice Sheet during the Last Interglaciation and implications for future change"

N. R. Golledge[1], P. U. Clark[2,3], F. He[4], A. Dutton[5], C. S. M. Turney[6,7,8], C. J. Fogwill[6,9,10], T. R. Naish[1], R. H. Levy[1,11], R. M. Mckay[1], D. P. Lowry[11], N. A. N. Bertler[1,11], G. B. Dunbar[1], A. E. Carlson[12]

[1]Antarctic Research Centre, Victoria University of Wellington, Wellington 6140, New Zealand
[2]College of Earth, Ocean, and Atmospheric Sciences, Oregon State University, Corvallis, OR, USA
[3]School of Geography and Environmental Sciences, University of Ulster, Coleraine, UK
[4]Center for Climatic Research, Nelson Institute for Environmental Studies, University of Wisconsin-Madison, Madison, WI, USA
[5]Department of Geoscience, University of Wisconsin-Madison, Madison, WI, USA
[6]Earth and Sustainability Science Research Centre, School of Biological, Earth and Environmental Sciences, University of New South Wales, Kensington NSW 2033, Australia
[7]Australian Research Council Centre of Excellence in Australian Biodiversity and Heritage, School of Biological, Earth and Environmental Sciences, University of New South Wales, Kensington NSW 2033, Australia
[8]Chronos 14 Carbon-Cycle Facility, University of New South Wales, Sydney NSW 2052, Australia
[9]School of Geography, Geology and the Environment, Keele University, Staffordshire ST5 5BG, UK
[10]School of Water, Energy and the Environment, Cranfield University, College Road, Cranfield, MK43 0AL, UK
[11]GNS Science, Avalon, Lower Hutt 5011, New Zealand
[12]Oregon Glaciers Institute, Corvallis OR 97330, USA

Contents of this file

1. Uncertainties associated with glacial isostatic adjustment
2. Uncertainty related to ocean temperature forcing
3. Figures S1 to S6
4. Tables S1 to S2

Uncertainties associated with glacial isostatic adjustment

One of the key advances we present in this paper, compared to our previous simulations for the LIG (Clark et al., 2020), is that our stiffer mantle parameterisation yields maximum ice loss earlier in the interglacial period, reaching a peak at 126 ka followed by subsequent ice sheet regrowth and sea level fall. This contrasts markedly with the former parameterisation that instead produced a long sustained peak sea-level contribution from 124 ka (Clark et al., 2020). The cause of these changes in timing and magnitude of mass loss is the mantle viscosity parameterisation, which in the new simulations is increased to 1.3×10^{20} Pa s, from the previous 1.0×10^{19}. Whilst this change allows a much closer fit to probabilistic interpretations of the Antarctic contribution to LIG GMSL (Kopp et al., 2009), we note that Kopp et al. (2009) caution the use of their ice volume projections on the basis that in their assessment they use a Gaussian distribution to represent a non-Gaussian prior. Furthermore we acknowledge that our isostatic parameterisation remains an area of considerable uncertainty and so provide further discussion of this part of our methodology here.

In the version of PISM that we employ here (v.0.7.1) we are limited to a 1-dimensional isostatic adjustment scheme that uses a single upper mantle viscosity and a single lithospheric rigidity value for the entire domain. It is therefore not possible for us to accomodate spatial heterogeneity in the isostatic model. This is common for most ice sheet models, and is directly comparable (in terms of simplification of approach) to previous LIG AIS simulations (Goelzer et al., 2016; DeConto & Pollard, 2016). Although those two studies employ different ice sheet models, both use the same radially-symmetric 1-dimensional isostatic scheme, based on Huybrechts and De Wolde (1999). According to Huybrechts (2002, p.205), this scheme yields bedrock deformation results beneath the Antarctic continent that are, '...close to those from a full visco-elastic treatment with mantle viscosities in the range 0.5-1.0 $\times 10^{21}$ Pa s'. Our value of 1.3×10^{20} Pa s represents a mantle rheology that is therefore 4 to 8 times less viscous than those studies, resulting in faster rebound in areas where ice is lost. In order to provide a broader context for these uncertain values, we collated inferences of upper mantle viscosity values from published studies (Table S2).

From Table S2 it can be seen that relatively weak Antarctic mantle exists beneath the Antarctic Peninsula, where values in the range 1×10^{18} to 1×10^{20} Pa s are common, and beneath the Amundsen Sea Embayment of West Antarctica, where inferences are mostly in the range 1×10^{17} to 1×10^{19} Pa s. Other sectors of West Antarctica, such as the southern Weddell Sea and the Siple Coast, are underlain by stronger mantle with viscosities typically in the range 1×10^{20} to 1×10^{21} Pa s. It is clear that the types of radially-symmetric isostatic models that our new experiments and other LIG studies have used do not fully capture the heterogeneity of asthenospheric properties inferred from geophysical observations and modelling studies. The primary impact of our use of a mantle viscosity that is stronger than inferred for some parts of West Antarctica would be the delayed rebound of bedrock following ice retreat. Figures S3 & S4 illustrate how sensitive our model is to this aspect of model parameterisation. However, we have employed what we believe to be a unique and rigorous tuning and validation procedure, in which we constrain our model parameterisation to values that allow the well-mapped Last Glacial Maximum (LGM) and present-day (PD) grounding line positions to be closely matched. If our isostatic scheme were too far from realistic values, we would either accelerate (if the mantle were too stiff) or delay (if the mantle were too fluid) retreat of the LGM ice sheet and we would not be able to reproduce PD grounding lines as well as we do (Fig. S4). To our knowledge, no LIG studies other than the present manuscript and our previous work (Clark et al., 2020) employ such an independent validation. On this basis we are confident that our model formulation is not only robust but is also closer to empirically-derived mantle rheologies than some previous studies. Nonetheless, we acknowledge that our solution in non-unique, and that further investigation would be valuable.

Uncertainty related to ocean temperature forcing

A further source of uncertainty in our simulations arises from the way in which we supply ocean thermal forcing to our modelled ice sheet. All LIG Antarctic Ice Sheet simulations have approached this problem differently. Goelzer et al. (2016) used a fully coupled ice-sheet–atmosphere–ocean model to simulate global climate and both the Greenland and Antarctic ice sheets in a consistent framework. They did not need to apply additional oceanic heat flux to drive West Antarctic Ice Sheet retreat. The spatial pattern of the LIG circum-Antarctic ocean temperature anomaly simulated by their model is not shown, however. DeConto and Pollard (2016) did not use model-based LIG ocean temperatures but instead used a present-day temperature map from the World Ocean Atlas (Levitus et al., 2012) to which they added spatially-uniform thermal anomalies (+3 to +4°C) un-

til ice sheet retreat was triggered. Sutter, Gierz, Grosfeld, Thoma, and Lohmann (2016) used a fully-coupled atmosphere-ocean general circulation model (AOGCM) to simulate LIG ocean temperature anomalies but also added spatially-uniform thermal forcing of +1 to +3°C in order to investigate the temperature threshold for collapse of West Antarctica. In our study we use a fully-coupled AOGCM to derive an oceanic forcing that is applied as an uncoupled transient forcing to our ice sheet model. We do not impose additional oceanic heat flux, but note that the ice–ocean feedback process (Menviel et al., 2010; Golledge et al., 2014) would have most likely increased subsurface warming and enhanced ice shelf basal melting. The spatial pattern of warming at the time of peak warmth (128.5 ka BP) at depths below the mixed layer in our CCSM3 simulations is shown in Figure S5. We observe strong warming offshore Dronning Maud Land (30°W to 30°E), strong cooling offshore Wilkes Land (80°E to 150°E), cooling in the Ross Sea embayment (170°E to 160°W), warming in the Amundsen Sea embayment and along the western Antarctic Peninsula (130°W to 60°W), and cooling in the Weddell Sea (60°W to 30°W). This distribution is qualitatively similar to results from Sutter et al. (2016) with the exceptions that they observe less cooling in the Ross and Weddell seas compared to our model, and less warming in the Amundsen Sea. Although there are no high-latitude ocean temperature proxies available to constrain circum-Antarctic temperatures south of approximately 50°S, we note that our simulated pattern of warming captures the same basic pattern as indicated for the current century in the multi-model mean of Climate Model Intercomparison Project Phase 5 (CMIP5) simulations, under Representative Concentration Pathway 8.5 (Naughten et al., 2018).

CCSM3 has been used to simulate a reasonable climate evolution of the deglacial surface temperature over Greenland, the surface ocean of the Southern Hemisphere, and over Antarctica (He et al., 2013; Buizert et al., 2014) as well as subsurface ocean temperature during Heinrich events in the North Atlantic (Marcott et al., 2011). We therefore have confidence in our simulated ocean thermal forcing prescription, but acknowledge that a different pattern of warming could produce a different pattern of ice retreat, with potential impacts on the AIS contribution to GMSL. However, our spatial pattern of mass loss is consistent with geologically-based inferences of ice sheet collapse in the Amundsen Sea sector (Carlson et al., 2021), with glaciological evidence of inland thinning in the southern Weddell Sea sector (Turney et al., 2020), and with geological signatures of enhanced ice sheet discharge offshore the Wilkes Subglacial Basin (Wilson et al., 2018). To-date, no conclusive records exist with which to either prove or disprove loss of ice from the Ross or Weddell Sea embayments during the LIG.

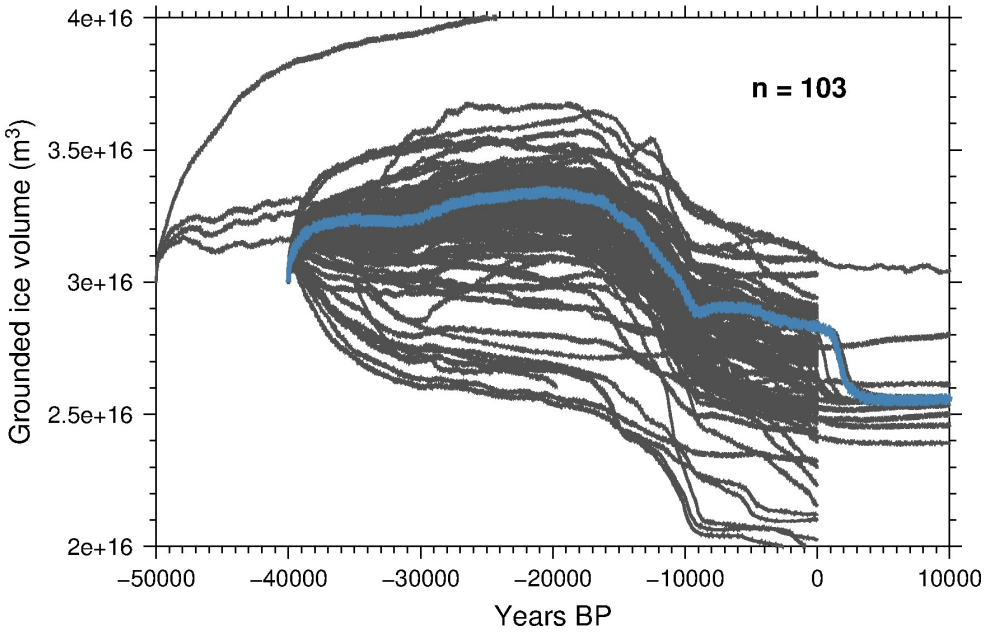

Figure S1. Evolution of grounded ice volume for the T1 experiment for 103 simulations that explore different parameterisations for flow enhancement factors, sliding exponents, substrate rheology, and grounding line schemes. Blue line shows the reference configuration (1.3e20 Pa s).

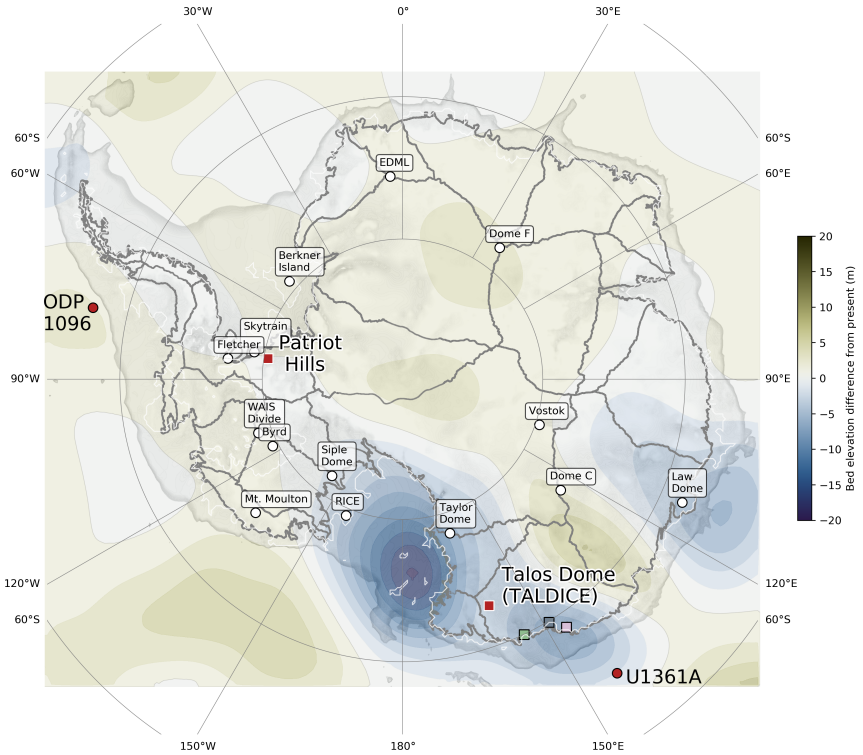

Figure S2. Bed elevation difference at 130 ka BP compared to present, based on linear interpolation of a Pliocene reconstruction of dynamic topography (Austermann et al., 2015). Changes in locations where the present-day ice sheet grounding line occurs are typically in the range -10 to +10 m. Grey lines show present-day boundaries of grounded ice catchments (Zwally et al., 2012). Patriot Hills blue ice area, Talos Dome ice core site, ODP1096 and U1361A marine sediment core locations and the three sites (coloured boxes) investigated in Figure 4 also shown. Labeled white squares identify ice core locations for which predictions of ice sheet change are presented in Figure S5.

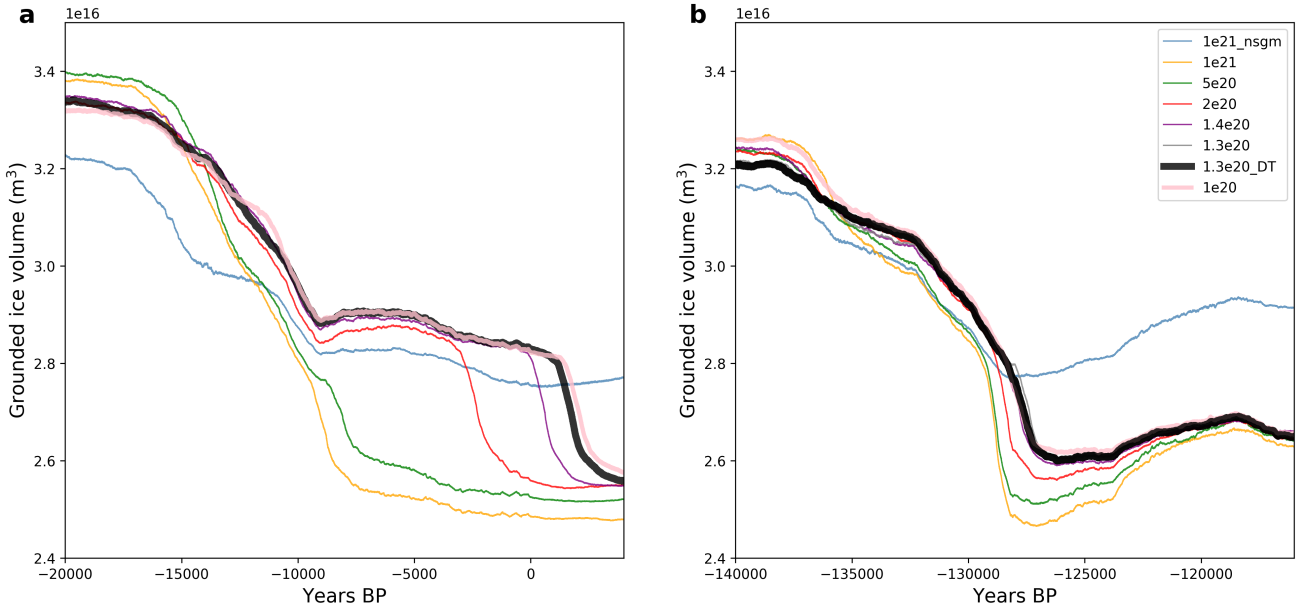

Figure S3. Impact of mantle viscosity variations on ice sheet evolution under T1 and T2 forcings. a) Timeseries of grounded ice volume for the last deglaciation (T1), used as a tuning experiment. Black line illustrates the reference experiment used as the basis for interpretations presented in this paper, pink line shows value used in previous simulations (Clark et al., 2020). Stiffer mantle viscosities lead to collapse of WAIS before simulated present-day ('Year 0') is reached. b) The same experiments as in a) but for the T2 climatology. Collapse of WAIS takes place earliest for stiffer mantle parameterisations, with only a very narrow range able to reproduce present-day grounding line extent as well as a multi-metre LIG contribution to sea level. Blue line in both panels illustrates a simulation in which the sub-grid grounding line scheme is turned off, effectively preventing the ice sheet from advancing or retreating adequately.

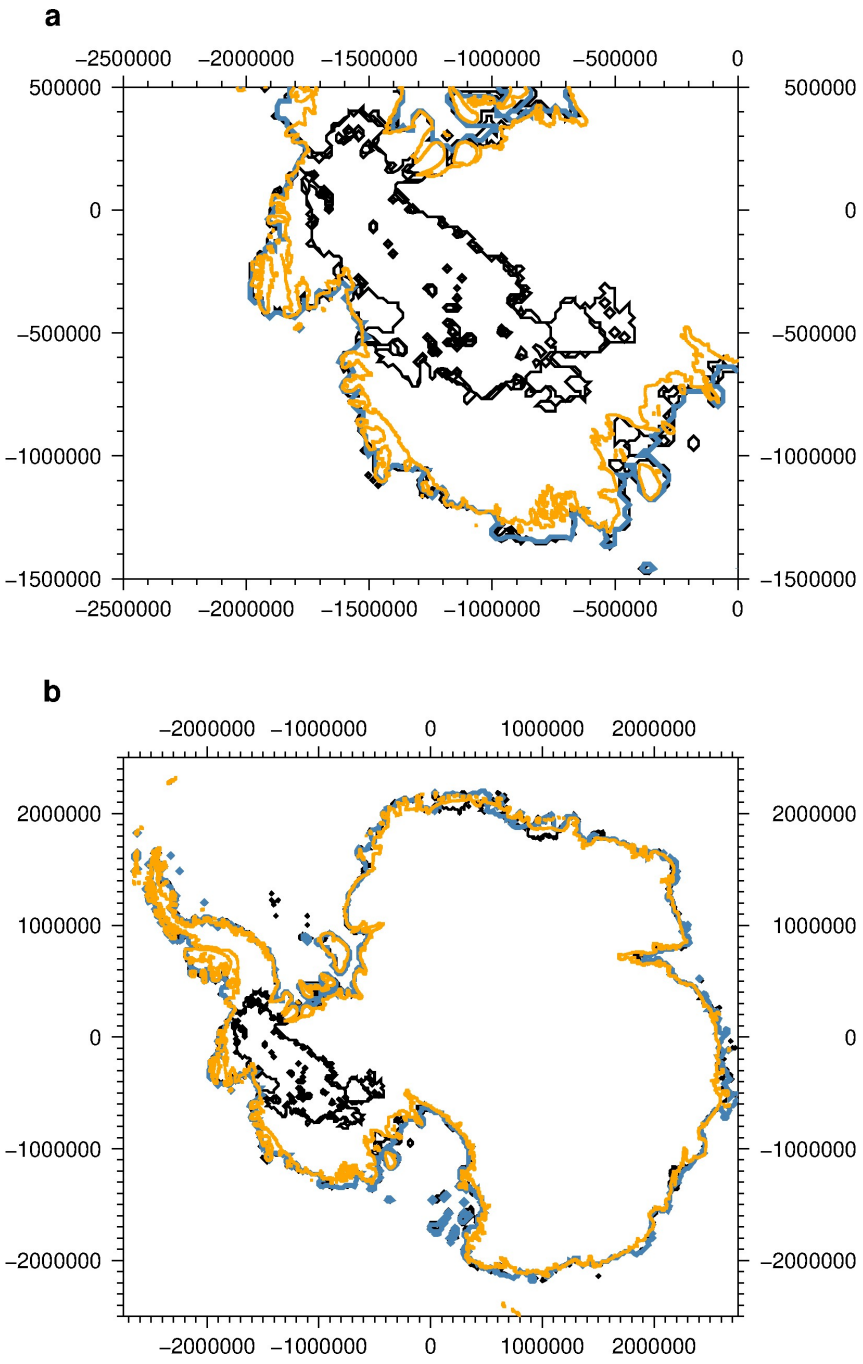

Figure S4. Impact of mantle viscosity variations on modelled present-day grounding line positions for a) West Antarctica, and b) the whole continent. In blue, the grounding line as represented by the reference configuration (1.3e20 Pa s) for the T1 experiment. Mantle viscosities greater than this lead to WAIS grounding line retreat to positions (black lines) further inland than the present-day observations (gold line) show.

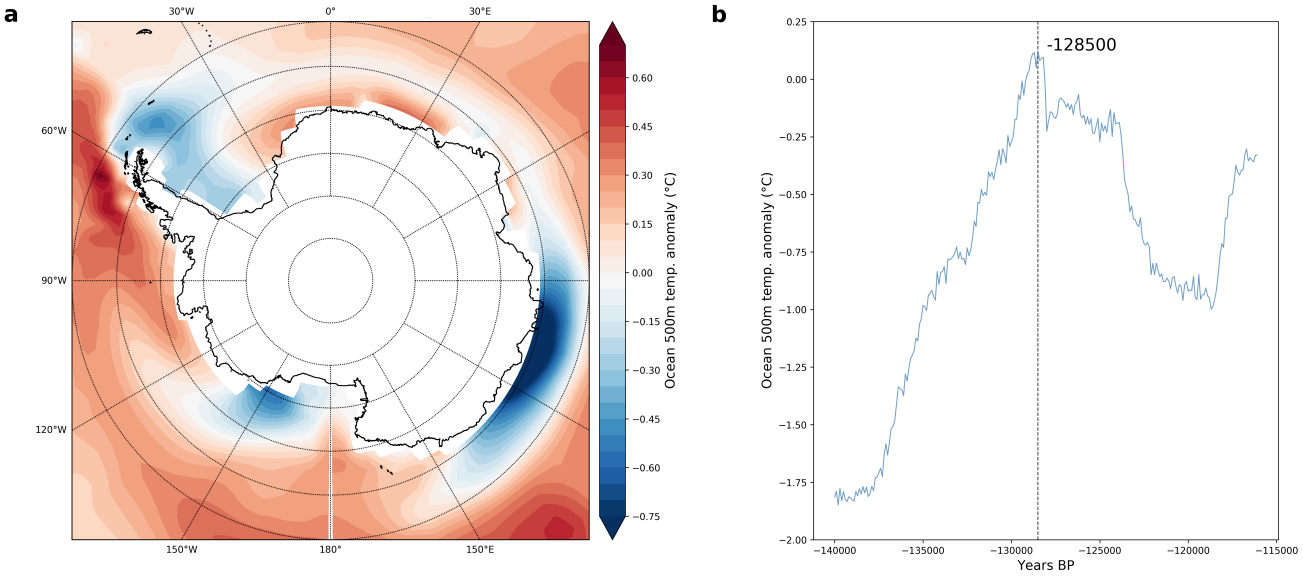

Figure S5. a) Ocean temperature (as anomalies from modelled present) simulated by CCSM3 for 500 m depth at the time of peak warmth (128.5 ka BP). Warming close to the Antarctic coast is evident along the western Antarctic Peninsula and into the Amundsen Sea Embayment, but cooler-than-present conditions prevail in the Weddell Sea and Ross Sea embayments. b) Zonally-averaged ocean temperature anomalies at 500 m depth from CCSM3. Vertical line shows peak warmth timeslice illustrated in a).

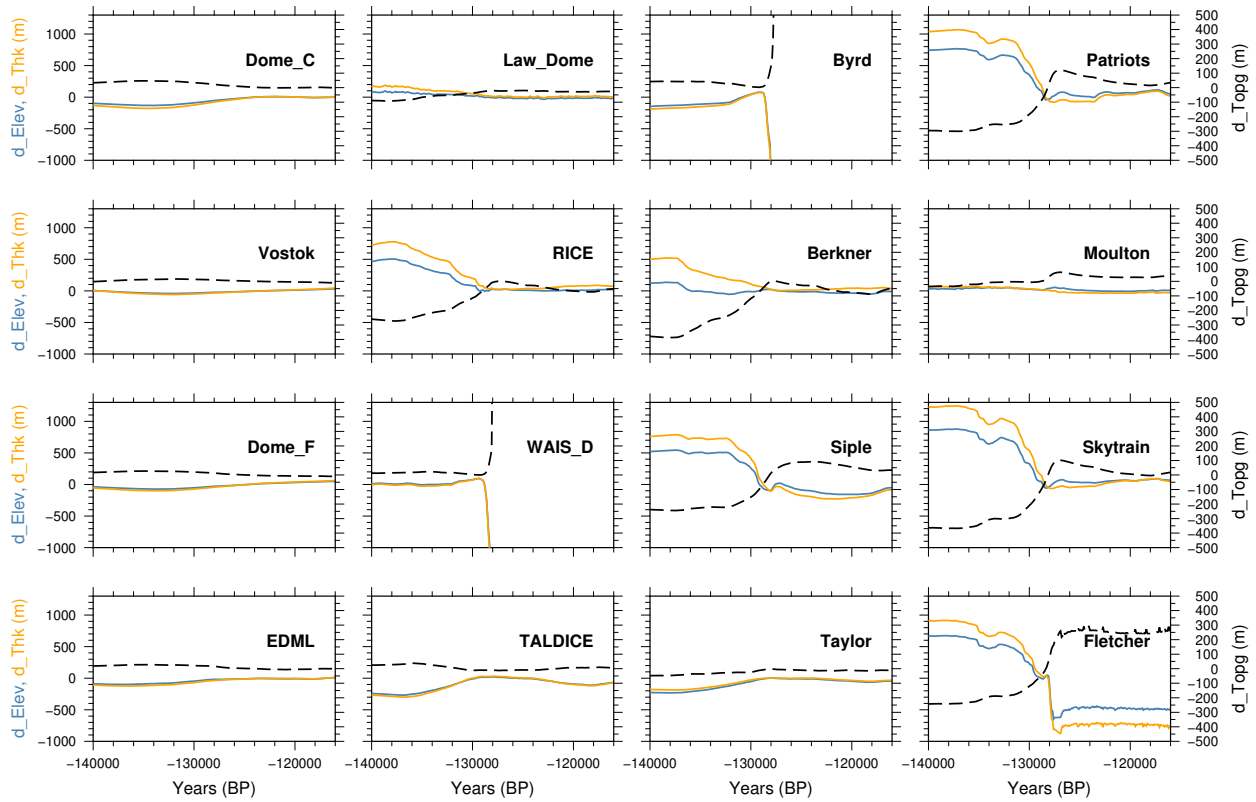

Figure S6. Changes in modelled ice thickness (gold), surface elevation (blue), and bed elevation (black) at each of the ice core sites shown in Figure 1c, shown as deviations from modelled present-day values at each site. Note the different scaling for the bed elevation changes (righthand axes) compared to that used for ice thickness and surface elevation (lefthand axes).

Table S1. Parameters used in the reference simulations for T1 and T2 experiments.

Parameter	Value	Units
PISM version	0.7.1	–
Domain x	289	cells
Domain y	249	cells
Vertical ice layers	121	–
Vertical bedrock layers	20	–
Computational box height	6000	m
z spacing (ice)	quadratic	–
z spacing (bedrock)	equal	–
shallow-ice approximation enhancement	1.75	–
shallow-shelf approximation enhancement	1.0	–
pseudo plastic q	0.25	–
eigen calving K	1e18	–
Thickness calving threshold	180	m
Grounding line scheme	subgrid	–
Till porewater overburden fraction	0.05	–
Atmospheric lapse rate	8	°C

Table S2. Inferences of upper mantle viscosity values for a range of locations and depths in West Antarctica. Where depth is unspecified, the value is assumed to apply to the full thickness of the upper mantle (approximately 660 km).

Study	Location	Depth	Viscosity
Simms et al., (2012)	South Shetland Islands	–	$1\text{x}10^{18}$ Pa s
Nield et al. (2014)	northern Antarctic Peninsula	–	$\leq 1\text{x}10^{18}$ Pa s
Samrat et al. (2020)	northern Antarctic Peninsula	above 400 km	$0.3 - 3\text{x}10^{18}$ Pa s
Samrat et al. (2020)	northern Antarctic Peninsula	below 400 km	$4\text{x}10^{20}$ Pa s
Ivins et al. (2011)	northern Antarctic Peninsula,	–	$4–7\text{x}10^{19}$ Pa s
Zhao et al. (2017)	central Antarctic Peninsula	–	$> 2\text{x}10^{19}$ Pa s
Wolstencroft et al. (2015)	southern Antarctic Peninsula	–	$1 - 3\text{x}10^{20}$ Pa s
Bradley et al., (2015)	southern Weddell Sea	–	$1\text{x}10^{21}$ Pa s
Barletta et al. (2018)	Amundsen Sea Embayment	65-200 km	$4\text{x}10^{18}$ Pa s
Barletta et al. (2018)	Amundsen Sea Embayment	200-400 km,	$1.6\text{x}10^{19}$ Pa s
Barletta et al. (2018)	Amundsen Sea Embayment	400-660 km	$2.5\text{x}10^{19}$ Pa s
Powell et al., (2020)	Amundsen Sea Embayment	–	$1\text{x}10^{17} - 1\text{x}10^{19}$ Pa s
Nield et al., (2016)	central Siple Coast	–	$\geq 1\text{x}10^{20}$ Pa s

References

Austermann, J., Pollard, D., Mitrovica, J. X., Moucha, R., Forte, A. M., DeConto, R. M., ... Raymo, M. E. (2015). The impact of dynamic topography change on Antarctic ice sheet stability during the mid-Pliocene warm period. *Geology*, *43*(10), 927–930.

Barletta, V. R., Bevis, M., Smith, B. E., Wilson, T., Brown, A., Bordoni, A., ... others (2018). Observed rapid bedrock uplift in Amundsen Sea Embayment promotes ice-sheet stability. *Science*, *360*(6395), 1335–1339.

Bradley, S. L., Hindmarsh, R. C. A., Whitehouse, P. L., Bentley, M. J., & King, M. A. (2015). Low post-glacial rebound rates in the weddell sea due to late holocene ice-sheet readvance. *Earth and Planetary Science Letters*, *413*, 79–89.

Buizert, C., Gkinis, V., Severinghaus, J. P., He, F., Lecavalier, B. S., Kindler, P., ... others (2014). Greenland temperature response to climate forcing during the last deglaciation. *Science*, *345*(6201), 1177–1180.

Carlson, A. E., Beard, B. L., Hatfield, R. G., & Laffin, M. (2021). Absence of West Antarctic-sourced silt at ODP Site 1096 in the Bellingshausen Sea during the last interglaciation: Support for West Antarctic ice-sheet deglaciation. *Quaternary Science Reviews*, *261*, 106939.

Clark, P. U., He, F., Golledge, N. R., Mitrovica, J. X., Dutton, A., Hoffman, J. S., & Dendy, S. (2020). Oceanic forcing of penultimate deglacial and last interglacial sea-level rise. *Nature*, *577*, 660-664.

DeConto, R., & Pollard, D. (2016). Contribution of Antarctica to past and future sea-level rise. *Nature*, *531*, 591-597.

Goelzer, H., Huybrechts, P., Loutre, M.-F., & Fichefet, T. (2016). Last Interglacial climate and sea-level evolution from a coupled ice sheet–climate model. *Climate of the Past*, *12*(12), 2195–2213.

Golledge, N., Menviel, L., Carter, L., Fogwill, C., England, M., Cortese, G., & Levy, R. (2014). Antarctic contribution to meltwater pulse 1A from reduced Southern Ocean overturning. *Nature Communications*, *(5)*, 1-10. doi: doi:10.1038/ncomms6107

He, F., Shakun, J. D., Clark, P. U., Carlson, A. E., Liu, Z., Otto-Bliesner, B. L., & Kutzbach, J. E. (2013). Northern Hemisphere forcing of Southern Hemisphere climate during the last deglaciation. *Nature*, *494*(7435), 81–85.

Huybrechts, P. (2002). Sea-level changes at the LGM from ice-dynamic reconstructions of the Greenland and Antarctic ice sheets during the glacial cycles. *Quaternary Science Reviews*, *21*(1-3), 203–231.

Huybrechts, P., & De Wolde, J. (1999). The dynamic response of the greenland and antarctic ice sheets to multiple-century climatic warming. *Journal of Climate*, *12*(8 PART 1), 2169–2188.

Ivins, E. R., Watkins, M. M., Yuan, D.-N., Dietrich, R., Casassa, G., & Rülke, A. (2011). On-land ice loss and glacial isostatic adjustment at the Drake Passage: 2003–2009. *Journal of Geophysical Research: Solid Earth*, *116*(B2).

Kopp, R. E., Simons, F. J., Mitrovica, J. X., Maloof, A. C., & Oppenheimer, M. (2009, December). Probabilistic assessment of sea level during the last interglacial stage. *Nature*, *462*(7275), 863–867. doi: 10.1038/nature08686

Levitus, S., Antonov, J. I., Boyer, T. P., Baranova, O. K., Garcia, H. E., Locarnini, R. A., ... others (2012). World ocean heat content and thermosteric sea level change (0–2000 m), 1955–2010. *Geophysical Research Letters*, *39*(10).

Marcott, S. A., Clark, P. U., Padman, L., Klinkhammer, G. P., Springer, S. R., Liu, Z., ... Schmittner, A. (2011). Ice-shelf collapse from subsurface warming as a trigger for Heinrich events. *Proceedings of the National Academy of Sciences*, *108*, 13415-13419.

Menviel, L., Timmermann, A., Timm, O. E., & Mouchet, A. (2010). Climate and biogeochemical response to a rapid melting of the West Antarctic Ice Sheet during interglacials and implications for future climate. *Paleoceanography*, *25*.

Naughten, K. A., Meisssner, K. J., Galton-Fenzi, B. K., England, M. H., Timmermann, R., & Hellmer, H. H. (2018). Future Projections of Antarctic Ice Shelf Melting Based on CMIP5 Scenarios. *Journal of Climate*, *31*, 5243-5261.

Nield, G. A., Barletta, V. R., Bordoni, A., King, M. A., Whitehouse, P. L., Clarke, P. J., ... Berthier, E. (2014). Rapid bedrock uplift in the Antarctic Peninsula explained by viscoelastic response to recent ice unloading. *Earth and Planetary Science Letters*, *397*, 32–41.

Nield, G. A., Whitehouse, P. L., King, M. A., & Clarke, P. J. (2016). Glacial isostatic adjustment in response to changing Late Holocene behaviour of ice streams on the Siple Coast, West Antarctica. *Geophysical Supplements to the Monthly Notices of the Royal Astronomical Society*, *205*(1), 1–21.

Powell, E., Gomez, N., Hay, C., Latychev, K., & Mitrovica, J. (2020). Viscous effects in the solid Earth response to modern Antarctic ice mass flux: Implications for geodetic studies of WAIS stability in a warming world.

Journal of Climate, *33*(2), 443–459.

Samrat, N. H., King, M. A., Watson, C., Hooper, A., Chen, X., Barletta, V. R., & Bordoni, A. (2020). Reduced ice mass loss and three-dimensional viscoelastic deformation in northern Antarctic Peninsula inferred from GPS. *Geophysical Journal International*, *222*(2), 1013–1022.

Simms, A. R., Ivins, E. R., DeWitt, R., Kouremenos, P., & Simkins, L. M. (2012). Timing of the most recent Neoglacial advance and retreat in the South Shetland Islands, Antarctic Peninsula: insights from raised beaches and Holocene uplift rates. *Quaternary Science Reviews*, *47*, 41–55.

Sutter, J., Gierz, P., Grosfeld, K., Thoma, M., & Lohmann, G. (2016). Ocean temperature thresholds for last interglacial West Antarctic ice sheet collapse. *Geophysical Research Letters*, *43*(6), 2675–2682.

Turney, C., Jones, R., McKay, N., Van Sebille, E., Thomas, Z., Hillenbrand, C.-D., & Fogwill, C. (2020). A global mean sea surface temperature dataset for the Last Interglacial (129–116 ka) and contribution of thermal expansion to sea level change. *Earth System Science Data*, *12*(4), 3341–3356.

Wilson, D. J., Bertram, R. A., Needham, E. F., van de Flierdt, T., Welsh, K. J., McKay, R. M., ... Escutia, C. (2018). Ice loss from the East Antarctic Ice Sheet during late Pleistocene interglacials. *Nature*, *561*(7723), 383–386.

Wolstencroft, M., King, M. A., Whitehouse, P. L., Bentley, M. J., Nield, G. A., King, E. C., ... others (2015). Uplift rates from a new high-density GPS network in Palmer Land indicate significant late Holocene ice loss in the southwestern Weddell Sea. *Geophysical Journal International*, *203*(1), 737–754.

Zhao, C., King, M. A., Watson, C. S., Barletta, V. R., Bordoni, A., Dell, M., & Whitehouse, P. L. (2017). Rapid ice unloading in the Fleming Glacier region, southern Antarctic Peninsula, and its effect on bedrock uplift rates. *Earth and Planetary Science Letters*, *473*, 164–176.

Zwally, H. J., Giovinetto, M. B., Beckley, M. A., & Saba, J. L. (2012). Antarctic and Greenland Drainage Systems. *GSFC Cryospheric Sciences Laboratory*, http://icesat4.gsfc.nasa.gov/cryo_data/ant_grn_drainage_systems.php.